Design and testing of a roto-translational shutter mechanism for planetary operation

Diego Scaccabarozzi [a,*], Bortolino Saggin [a], Edoardo Alberti [b]

[a] Politecnico di Milano, Polo Territoriale di Lecco, Via M. d'Oggiono 18/a, 23900 Lecco, Italy
[b] Micos Engineering GmbH, Dübendorf (ZH), Switzerland

1. Introduction

Though not commonly made, roto-translational motion would be often a desired characteristic for shutter mechanisms for space borne instruments, mainly on those devoted to planetary surface operation. For these devices opening of instrument field of view (FOV) can be achieved by a rotation while cover translation would allow to generate a pressure on a compliant gasket around the instrument entrance window. This is the best way to achieve the sealing against external contamination caused by dust or condensation, since in comparison with purely rotary covers, that achieve sealing during the last phase of the rotation, the advantage of a linear motion lays in the possibility to generate a uniform pressure distribution over the seal.

Apart from the front door mechanism of OSIRIS-Rosetta experiment [1], in literature no solutions about this kind of combined movement were found. OSIRIS mechanism however was not scalable to our case since the design had to cope with an allowed total mass ten times lower than OSIRIS one. Our instrument mass budget was 1 kg [2], therefore a new shutter/calibrating mechanism had to be conceived and designed.

Cover rotation is provided by out of plane cams which work faced and axial movement is possible since the shutter is guided by an external fixed cam. The most remarkable characteristics of the conceived mechanism are its compactness and lightweight. It suffices to say that the overall mass was lower than 30 g. The mechanism is

* Corresponding author. Tel.: +39 34 148 8810.
E-mail address: diego.scaccabarozzi@mail.polimi.it (D. Scaccabarozzi).

powered by a commercial gearbox motor Portescap R10 with a nominal output torque of 0.1 Nm, a temporary working with 0.15 Nm limit and low mass and size. This off the shelf motor was not compatible with space application because of the materials outgassing characteristics, therefore it was selected as temporary solution for the breadboard development phase. Moreover, the operating temperature range declared by the motor manufacturer has a lower limit of $-40\ ^{\circ}C$, therefore not compatible with the required operating temperature of about $-80\ ^{\circ}C$. A specific re-design of the motor unit to achieve compliance with environmental requirements was planned in the cover development plan.

The mechanism development is presented in the following: Section 2 describes design requirements and constraints, mechanism working principle and the cover and mechanism designs; performance and environmental tests are presented in Section 3 and the paper is eventually concluded in Section 4.

2. Mechanism design

2.1. Design constraints

The mechanism was developed for the Mars Infrared Mapper (MIMA), a miniaturized infrared spectrometer selected for mounting on the 2007 configuration of the ExoMars high-mobility rover devoted to Mars surface observation. Beside complexity owing to the double motion, design challenge was increased by strict mass and size constraints [2]. Moreover minimum rotation of 60° was required to achieve the instrument unobstructed FOV.

Expected mechanical environment was characterized by high acceleration levels:

- a quasi-static acceleration of 670 m/s^2 corresponding to the landing shock; and
- a sine acceleration amplitude of 330 m/s^2 was specified within the 30–100 Hz frequency range; and

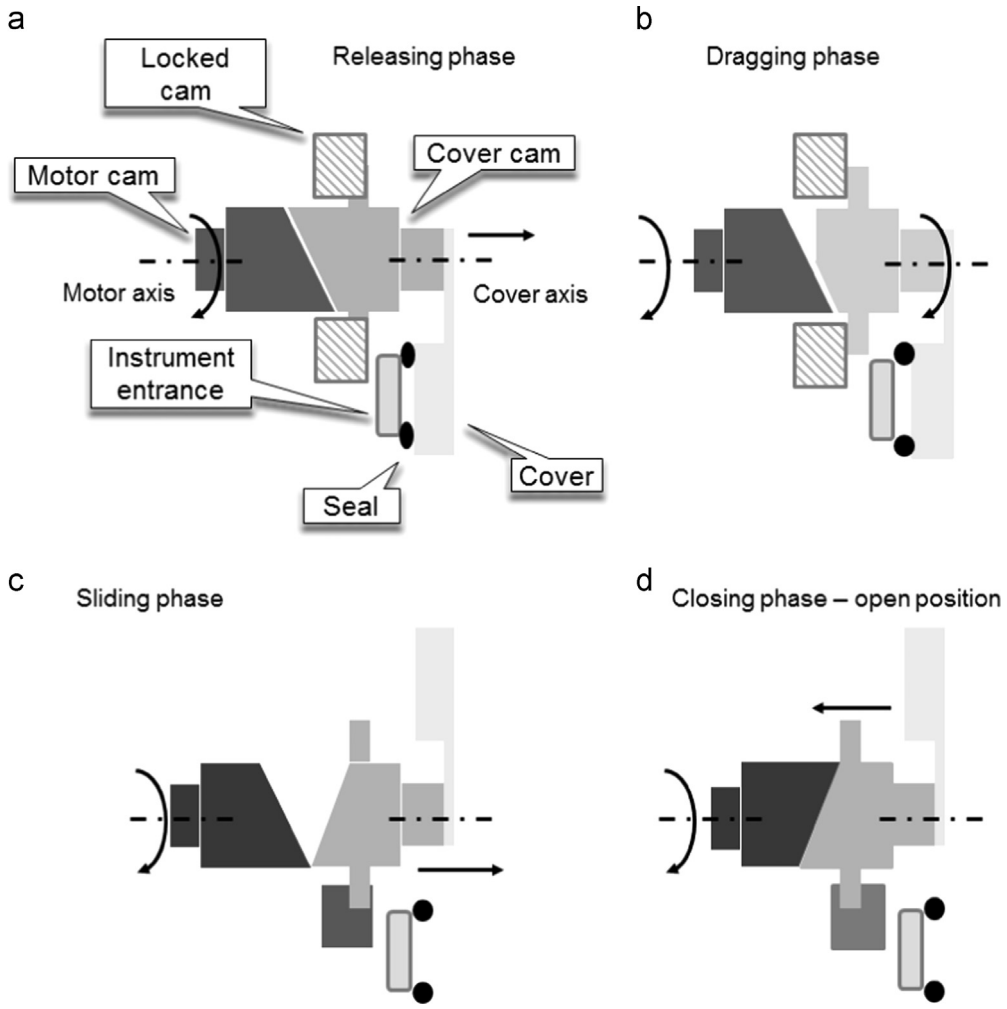

Fig. 1. Mechanism working principle (a) System starts from a fully closed position with zero axial relative distance between motor and cover cams. Motor starts rotating and cams slide up to cover cam release. (b) Dragging starts and cover rotates. (c) Cover cam reaches the open position and sliding process restarts. (d) System backs to zero axial displacement and stable open position is provided.

- random excitation corresponding to an rms acceleration of 170 m/s^2 was specified between 20 and 2000 Hz.

Thermal environment was harsh as well since the mechanism had to work within the $-70 \div 30$ °C temperature range and survive the $-120 \div 120$ °C in non-operating state. This posed strong limitations about materials usage and outgassing phenomena.

2.2. Mechanism working principle

The mechanism is essentially made up by three cams, hereafter named motor cam, cover cam and locked cam. The motor cam is rigidly connected to the motor thus can only rotate. It is manufactured with a sinusoidal out of plane shape and interacts with the cover cam that is rigidly linked to the mechanism cover. The last cam can both translate and rotate and its motion is controlled by external radial "teeth" of the third locked cam. Sketch of Fig. 1a shows mechanism in entrance window sealing configuration.

Expected motion has four phases: at the first step motor cam rotates and the cover cam can only translate along its rotating axis. This releasing phase is necessary to unload the entrance sealing element (Fig. 1b).

Cams sliding is possible since cover cam rotation is prevented by the locked cam. Once the required displacement to unlock the cover cam is reached, the cover starts rotating thanks to dragging coming from the friction between motor and cover cams. This phase extends up to complete release of the instrument FOV. Once the required angle is reached, the cover rotation is prevented again by the locked cam so cams slipping restarts and the cover moves axially up to the maximum displacement, as shown in Fig. 1c.

Motor cam however rotates until cover returns to the zero axial displacement so that a stable "open position" is achieved (Fig. 1d). Open position is stable since any undesired rotations caused by vibration or external forcing, are prevented by the locked cam stops. To close the mechanism and seal the instrument entrance window again, motor is actuated in the inverse direction so that all motion phases are backwards retraced.

It is worth noticing that cover cam would continuously slide without rotating the cover arm in case the cover was stuck owing to a resistant torque significantly larger than expected, and in particularly larger than that provided by the friction between the cams. Thus, in order to increase mechanism reliability a safety system has been implemented. This system provides a stop between motor and cover cams after a relative sliding of 270° to apply the full actuating torque once cover cam is positioned at its maximum axial elevation. In this emergency mode, the cover rotation occurs and motor stops once instrument FOV release is achieved. Thus observation would still be possible (as long as the motor torque is enough to overcome the unexpected friction increase) although the axial movement capability is lost along with the dust tightness of the cover.

2.3. Cover thermo-mechanical design

The cover is of primary importance since it has to provide optics protection from external contamination and the calibration sources for the spectrometer [3]. Cover

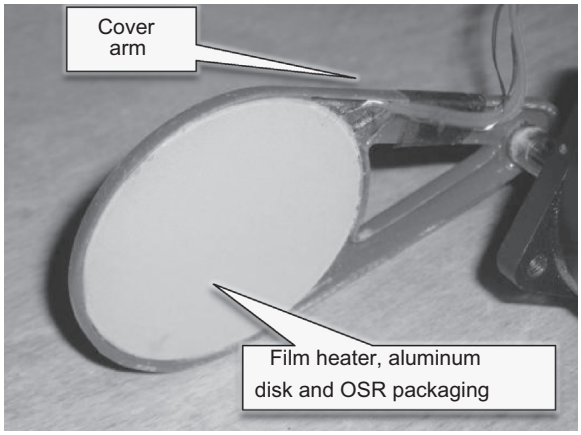

Fig. 2. Shutter/calibration cover assembly.

inner surface is the instrument calibration body, made by a film heater (0.5 W overall power dissipation) bonded to an aluminum disk with an optical solar reflector (OSR) on the top, that is mounted on a glass-fibre reinforced epoxy (GRE) structural arm. GRE was chosen because of its lightness, low thermal conductivity and mechanical strength. A picture of the cover assembly is shown in Fig. 2.

To evaluate the cover mechanical strength and stiffness requirements fulfilment, finite element (FE) analyses were performed by means of PTC-Pro/Engineer Mechanica software. In the mechanical FE model the calibration arm is fully constrained near the connection to mechanism shaft and is loaded by the expected acceleration of 670 m/s^2 along each of three coordinate axes. The orthogonal direction with respect to the calibration surface has proven to be the worst case though the loading should not act in that direction according to the instrument mounting configuration. Anyway, this condition has been used as worst case to provide full compliance whatever the instrument mounting plane.

Moreover a thermal model, developed with ESATAN TMS software and refined with PTC Pro/Engineer Mechanica, computed temperature distribution over the calibrating surface with the calibration heater switched on and the cooling due to convection with Martian atmosphere, represented as carbon dioxide at 10^3 Pa pressure. Temperature at the cover mounting interface was set at -70 °C, while in order to simulate the worst-case operative scenario, convective exchange was modelled considering 20 m/s wind speed and an atmosphere temperature of -70 °C.

Mechanical and thermal properties of the materials used to develop cover and mechanism FE models are summarized in Table 1.

Fig. 3shows Von Mises stresses due to quasi-static loading while temperature distribution over the cover surface is reported in Fig. 4,

Fig. 3 shows that the maximum VM stress computed over the entire model is close to 80 MPa at the cover arm constraint. In accordance to ECSS standards [4,5], margin of safety (MS) was computed:

$$MS = \frac{\sigma_{ADM}}{FOS^{*}\sigma_{MAX}} - 1, \tag{1}$$

Table 1
Material properties of the cover model.

Material property	Unit	Aluminum 7075 T3	Glass fibre-epoxy	Vespel SP 22	Stainless steel AISI 4140
Young modulus	GPa	70	70	2.4	205
Density	kg/m^3	2800	1500	1400	7850
Poisson ratio		0.33	0.20	0.41	0.29
Ultimate tensile strength	MPa	570	400	51.7	800
Yield Tensile Strength	MPa	380	n.a.	n.a.	600
CTE 10^{-5}	°C^{-1}	2.3	0.3	2.1	1.6
Thermal conductivity	W/(°C m)	156	0.04	0.35	16

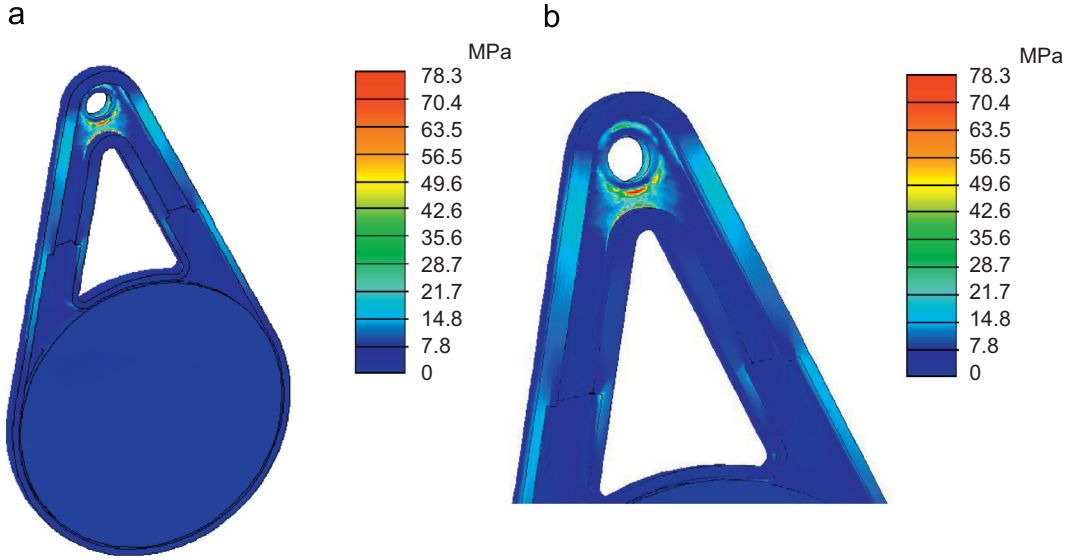

Fig. 3. (a) Von Mises stress over the calibrating cover in quasi-static loading analysis (b) Zoom of the stress distribution near cover attachment.

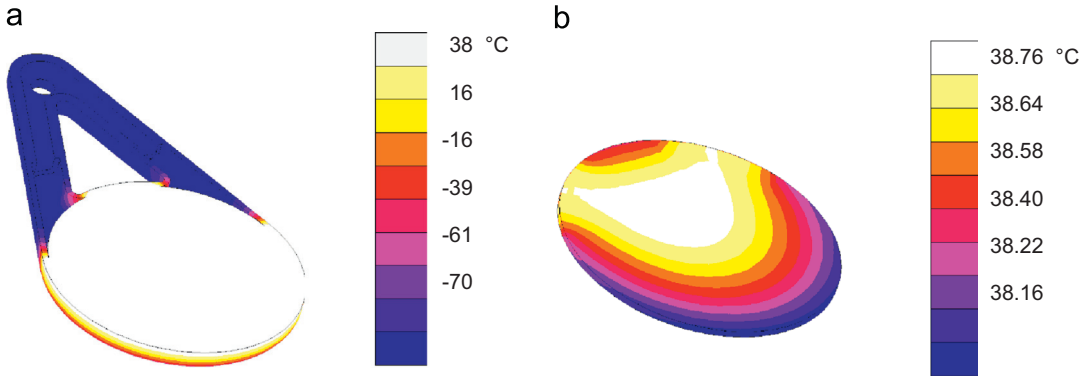

Fig. 4. (a) Temperature distribution of the calibrating cover (b) Detail of the calibrating surface temperature distribution.

where σ_{MAX} and σ_{ADM} are, respectively, the maximum and the yield Von Mises stresses, FOS is the safety factor against yield condition, set at 1.5 for quasi-static loading. Computed MS resulted in 2.3, acceptable result being MS larger than zero.

Thermal analysis provided two main outcomes: cover surface reaches a mean temperature of 40 °C with a power heater of 0.5 W. Calibrating surface temperature distribution varies within 0.6 °C range, this leads to acceptable results in terms of achievable radiometric accuracy [3]. Testing in normal atmospheric conditions has been used to validate the thermal model predictions about temperature uniformity over the calibrating surface [6].

2.4. Mechanism design

2.4.1. Elastic element and friction definitions

An elastic element has to be used to create an adequate contact force between motor and cover cams and assure the compression of the seal. Contact with the seal avoids

the cover unlocking during launch and landing, critical for the high mechanical loading. Required axial load F_p to keep cover in closed position can be computed as:

$$F_P = m \ \text{FOS} \ a, \tag{2}$$

where a is the quasi-static acceleration expected at mars landing shock, FOS is safety factors derived from ESA mechanism design standards [5], m is the overall cover mass (15 g). Smalley CM20-L2 [7] element was chosen for our purposes because of its lightness and small size, i.e. 19 mm external diameter, a free height of 3 mm and nominal spring rate of 35 N/mm.

Cams friction determines motion phases, i.e. it has to be overcome during sliding while it assures torque transmission when cover is unlocked and the rotation is allowed; friction depends on cams materials and environmental conditions. DuPont Vespel® polymide SP22 [8] was chosen for the motor cam while aluminum Al7075-T3 for the motor and locked cams. Vespel provides an acceptable compromise between mechanical resistance (yield stress of 50 MPa), outgassing properties, CTE (close to the aluminum one) and friction, with static and dynamic coefficients of 0.27 and 0.24, respectively. CTE matching has a key role to reduce thermal stress due to different materials expansion that is critical because of the wide working temperature range.

2.4.2. Cams shape design

Mechanism strokes can be freely chosen in order to minimize mechanism size and assure cams shape manufacturing feasibility. Axial displacement of 0.5 mm was chosen to define cover translation and seal preloading as well, while 1 mm was set as maximum distance between motor and cover cams before opening position is reached. As mentioned above, meshed elements shapes are symmetrical and sinusoidal so that intended smooth profile reduces vibration during motion phases. Cam shape was defined computing the actuating force and resistance due to friction. Worst condition happens once the maximum axial displacement is reached. In that condition cams' slipping has to be ensured to complete the movement. Sketch of Fig. 5 shows interaction between simplified shapes and provides the contact plane reference system where tangential and normal forces were computed:

$$\begin{aligned} F_t &= F_a \ \cos(\alpha) - F_s \ \sin(\alpha) \\ F_n &= F_a \ \sin(\alpha) + F_s \ \cos(\alpha) \end{aligned} \tag{3}$$

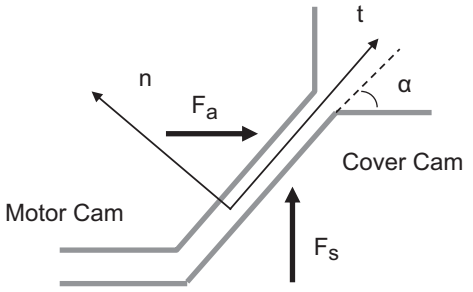

Fig. 5. Scheme of the contact between cams shapes.

where F_s and F_a are, respectively, the elastic and actuating forces and α is the shape angle. Motion is possible only if the motor torque is enough to win the resistance due to friction:

$$F_t \geq F_n{}^* \mu_s \tag{4}$$

μ_s is the friction coefficient of aluminum and vespel contact. According to [5], spring rate has to be increased by 20%. Normal and tangential forces can be computed by means of Eq. (3) that gives the maximum angle α that satisfies inequality (4). Nominal actuating torque was set to 50 N/mm to be compatible with miniature motors. Because of size constraints, mean cam radius was limited to 7 mm and by means of Eq. (4) maximum cam shape angle was computed (10°).

Gravity generates a resistant torque that depends on the position of the mechanism with respect to the gravity acceleration vector. To warrant working in both Mars and Earth conditions, the Earth gravitational acceleration was used for the mechanism sizing. Actuating torque is provided by an off the shelf brushed motor from Portescap [9] with nominal torque of 100 Nmm and maximum of 150 Nmm for limited time. Thus torque margin was eventually evaluated:

$$\eta = C_{adm} / C_{\max}, \tag{5}$$

where C_{adm} and C_{max} are respectively admissible and resistant torques. Torque margin resulted in 2.7, value compliant to ECSS standards.

Adhesion limit verification was also performed. Pressure limit for the SP22 material was not defined by manufacturer so it was computed by scaling the axial fatigue limit of the SP21 (46.2 MPa). This was the only information available. Adhesion test pressure limit of 29.4 MPa was obtained. Test was performed in the worst loading condition identified by 1 mm cover displacement leading to an external load of 50 N due to spring compression. The Hertzian theory was used to compute the maximum pressure at the contact:

$$\begin{aligned} P_{\max} &= \frac{2F_s}{\pi b l} \\ b &= \sqrt{\frac{2F_s \left(1-\upsilon_1{}^2\right)/E_1 + \left(1-\upsilon_2{}^2\right)/E_2}{1/d_1 + 1/d_2}} \end{aligned} \tag{6}$$

F_s is the contact force, d_1 and d_2 are cylinders diameters and l is the cylinders thickness. Test is passed if maximum pressure P_{max} is lower than adhesion limit, so Eq. (7) can be exploited to define the minimum cams thickness that prevents from adhesion. It was found that 5 mm thickness satisfies the adhesion requirement. The resulting cam geometry is summarized in Table 2 while motor and cover cams are shown in Fig. 6a and b, and picture of locked cam teeth is provided in Fig. 6c.

2.4.3. Mechanism auxiliary parts

Here a brief description of all the mechanism elements is presented. Design was guided by the requirement of minimizing axial and radial size, assure easy mounting and spring preloading regulation. Fig. 7 shows a section of the mechanism assembly.

An aluminum plate (top plate) and a vespel bushing interact through an SKF AXK 0821TN axial bearing with the motor cam. The locked cam is mounted to the supporting frame by means of three attachments feet at 120°. The cover cam is rigidly connected to the cover through an aluminum shaft radially guided by vespel bushings. Spring provides required cam contact and is mounted between cover shaft and SKF AXK 0515 TN axial bearing. Finally an aluminum plate (bottom plate) is used to provide required spring preloading. Cover is mounted at the shaft end by means of a bolt, thus allows cover angular position adjustment to fit entrance window sealing once mechanism is mounted on the instrument. As shown in Fig. 7 small size was achieved being mechanism envelope limited to 27.2 mm in the axial direction with a 24 mm diameter.

Table 2
Cam shape parameters.

Mean Diameter [mm]	14
Thickness [mm]	5
Axial height [mm]	1
Shape angle [°]	10

2.4.4. Thermo-mechanical design

A FE model was built to evaluate mechanism mechanical resistance under quasi-static loading. Mechanism parts were fully modelled, while the calibration cover was represented only as an inertial equivalent. Quasi-static excitation of 670 m/s^2 was applied in three directions, i.e. along the cover rotation axis and the others in a plane normal to it. Fig. 8a shows Von Mises stresses resulting

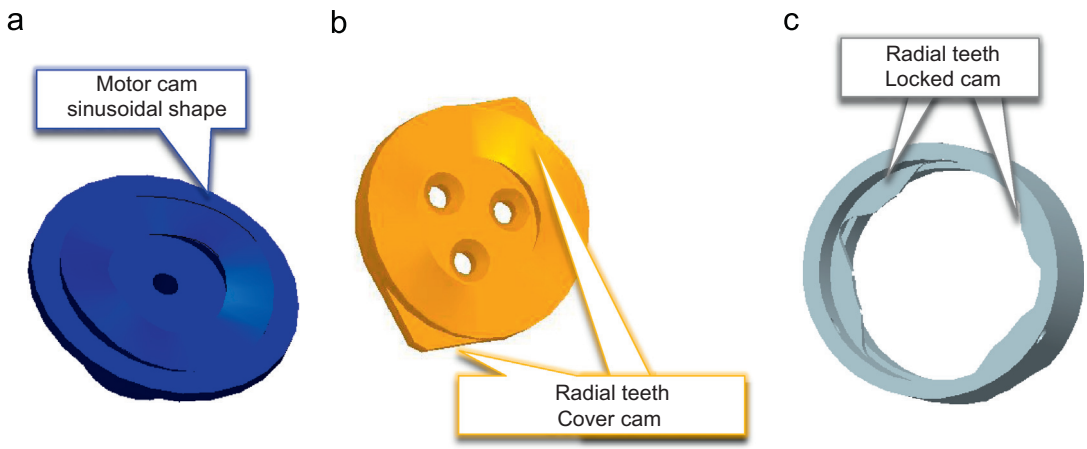

Fig. 6. Mechanism cams 3D models (a) Motor cam (b) Cover cam (c) Locked cam.

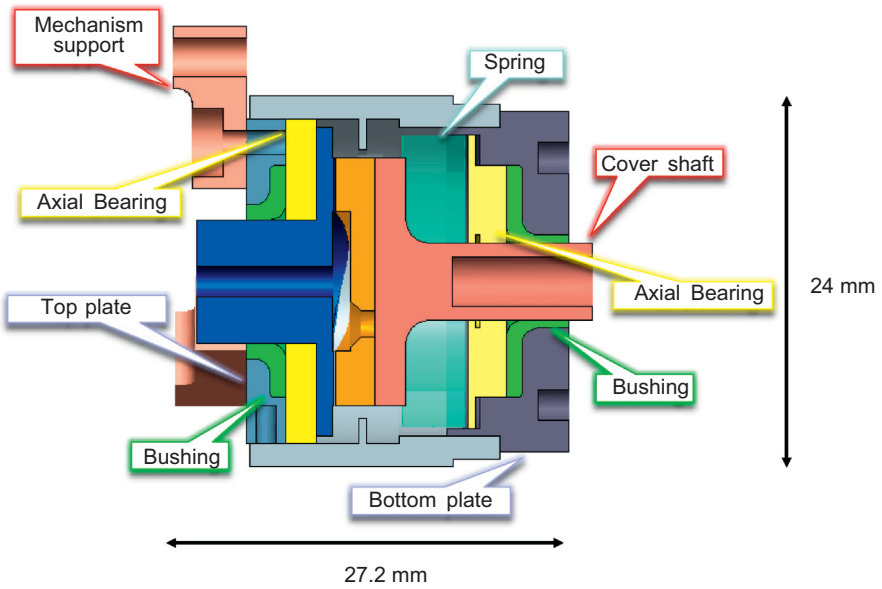

Fig. 7. Picture of a mechanism section. Axial and radial dimensions are, respectively 27.2 and 24 mm.

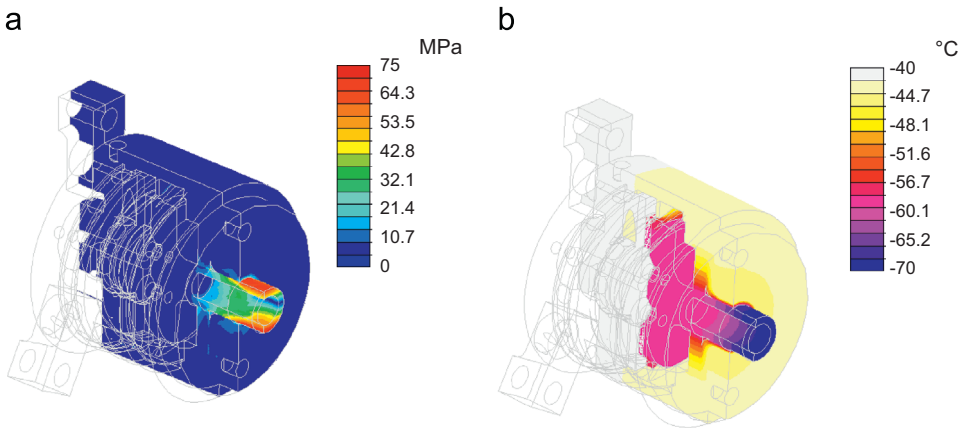

Fig. 8. Sections of the mechanism FEM models (a) Von Mises stresses due to the static analysis with 670 m/s^2 quasi-static loading along the cover rotation axis. (b) Temperature distribution over the mechanism in the cold operational condition.

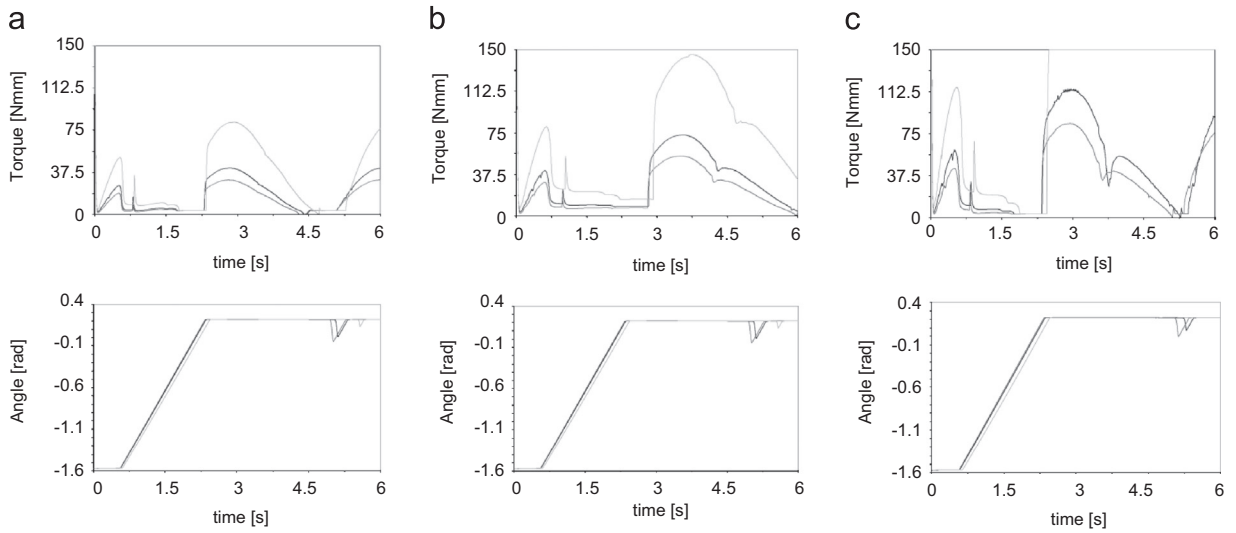

Fig. 9. Torques and cover rotation resulting from sensitivity study. Light grey, dark grey and black curves show torques and rotations, respectively, with 70 N/mm, 26 N/mm and 35 N/mm. (a) Torques and rotations with nominal friction (b) torques and rotations with lowest friction (c) torques and rotation with highest friction.

from worst case loading, i.e. with the load acting along the cover rotation axis. Highest stress level was detected on the cover shaft although computed stress is five times lower than material yield strength. Minimum MS resulted in 0.6 for the vespel material whose maximum stress of about 10 MPa was located at the cover cam radial teeth.

A FE thermal model was developed in order to determine the thermal gradients through the mechanism that could jeopardize its functionality in the expected thermal environment. Interface links temperature was set to -40 °C and convection with Mars atmosphere was added at the cover and shaft. Fig. 8b shows thermal analysis result. Maximum gradient was detected on the cover shaft where temperature ranges between $-70 \div -60$ °C. Thermo-elastic analysis with computed temperature distribution proved the mechanism mechanical resistance to this scenario.

2.4.5. Friction sensitivity analyses

A multi body model was built to verify mechanism kinematics and required torque in nominal working conditions. Spring stiffness and friction are critical for the mechanism working so a sensitivity analysis was performed in the following cases:

- nominal condition with 0.27 and 0.24 as static and dynamic friction coefficients; and
- low friction with static and dynamic coefficients set to 0.135 and 0.12; and
- worst condition with static friction of 0.4 and dynamic one at 0.3.

In each condition spring stiffness was set at 26 N/mm and 70 N/mm beside the nominal value of 35 N/mm.

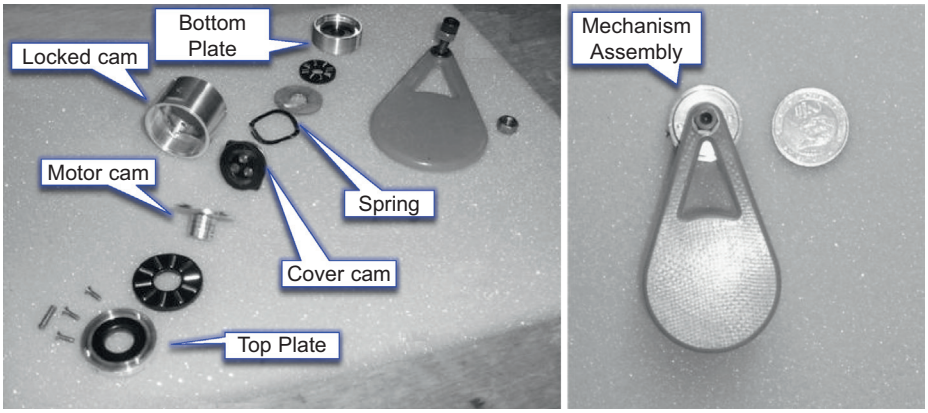

Fig. 10. Mechanism assembly breakdown.

The model was developed by means of MSC Adams multibody software. Model included cams, bushing and calibration cover and contacts between them. Fig. 9a shows motor torques and cover rotation in nominal working condition.

Computed torque with nominal stiffness shows a peak of 42 Nmm once releasing phase is completed, and then reduces at about 15 Nmm to drag the cover. Maximum torque is about 70 Nmm once maximum axial displacement is reached. Time required to complete the movement is 6 s with the required cover rotation of 1.85 rad. Displacement of Fig. 9a shows that near 5 s the cover rotates back (0.2 rad in the case of 35 N/mm); this is caused by the gravity action that exceeds the friction torque. Even with this unwanted motion the cover is correctly closed. The largest spring stiffness causes a higher resistance that requires the motor to work in the temporary working range for about 1.3 s. Moreover, increasing spring stiffness reduces cover backward movement in fact 0.1 rad rotation angle is computed in the case of 70 N/mm.

Fig. 10b provides simulation results with the lowest friction. Motor torque remains lower than 100 Nmm even in the case of maximum stiffness and resistance. Moreover, cover backwards rotation increases up to 0.625 rad and remains constant varying the spring stiffness.

Fig. 10c shows torque and rotation in the worst case. Torques increases due to the friction so that more effort is needed to assure the movement, even in the case of lowest spring stiffness. In the case of 70 N/mm, resistance during the slipping at the maximum axial displacement becomes so large that movement cannot be completed. For what concern the cover rotation, it can be noticed that backward cover movement is still present and is close to what computed in the nominal condition.

Model simulations showed that expected mechanism movement can be achieved in all cases except for the one in which the stiffness and friction are both maximal since the torque provided by the motor is not enough to complete the opening.

A backward movement caused by Earth gravity was identified. This happens when the cover is completing the closing phase and cams axial distance is close to 0.5 mm, i.e. half of the cams height. The irregular movement does not impair cover functionality but can be removed if the axial distance corresponding to the stable open position reduces. This is obtained by modifying the axial displacement at the releasing phase so that 0.8 mm is required to unlock the rotation.

Locked cam teeth thickness increases but the stable open position is reached at an axial displacement lower than before, theoretically 0.2 mm instead of 0.5 mm, and backwards movement is avoided. This minor modification is effective in terms of rotation but requires larger torques to complete the movement, about 30% more than before.

Eventually to keep a satisfactory margin of safety about the motor torque, 0.5 mm displacement was selected as baseline solution for the mechanism breadboard development. Moreover, gravity on Mars is expected to be one third of the earth one, so the unwanted rotation would be less relevant.

3. Prototype testing activity

Mechanism parts were manufactured and assembled to realize the prototype shown in Fig. 10.

The prototype was tested to assess opening and closing torques, verify actuation within the expected temperature range and confirm mechanism mechanical resistance within mechanical environment.

3.1. Torque measurement condition actuation

In order to verify mechanism working and validate multibody modelling the mockup was actuated and required torque was measured. Fig. 11a shows the test setup with the motor (housed in a cylindrical aluminium frame), a torque sensor DR 2112 Lorentz Messtechnik GmbH with 1 Nm full scale and 0.1% accuracy, and the mechanism mockup.

Measured torque is shown in Fig. 11b. Maximum was reached at the releasing phase, about 55 Nmm, while dragging phase required 40 Nmm. The final cams slipping showed a torque of about 80 Nmm.

Results showed an increase of required effort in all movement phases with respect to the computed torques. Explanation was found in axial bearings irregular working that caused friction increase; the issue that would be

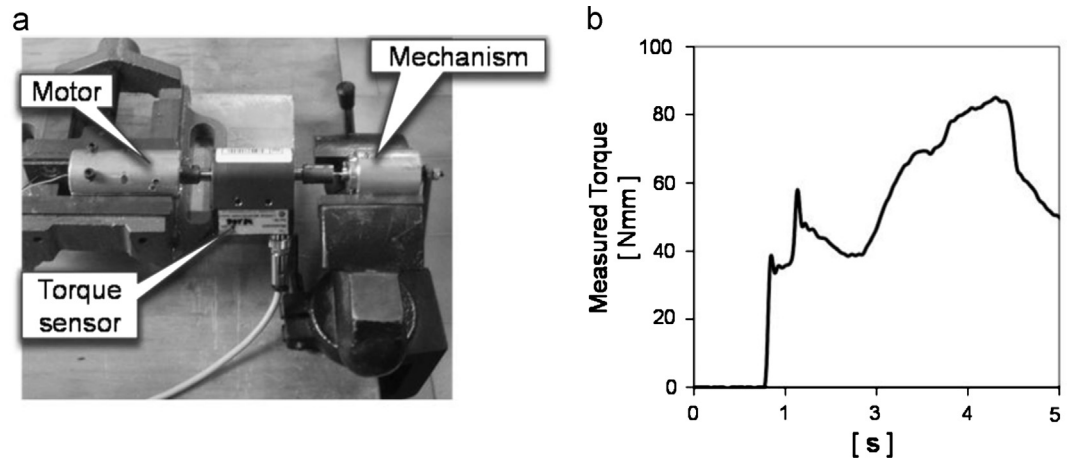

Fig. 11. Torque measurement setup.

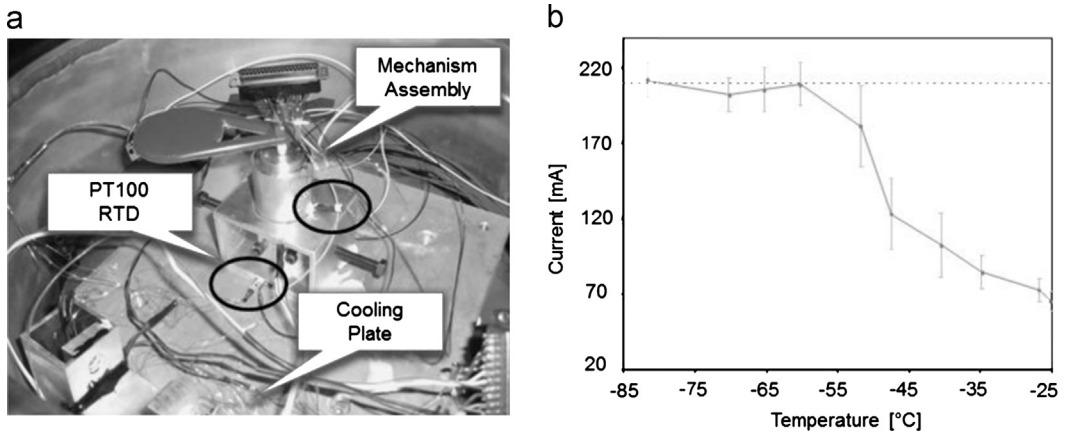

Fig. 12. (a) Setup to measure mechanism performances at low temperature (b) Trend of the current provided to the motor, vs temperature. Uncertainty bands are shown with 1σ width.

overcome by enhancing bearing guides manufacturing tolerances. Main result was that the motor provides enough torque to complete the movement, with 20% residual torque respect to the maximum admissible continuous value and about 50% with the respect to the maximum value on the temporary working range. Moreover rotation did not show anomalies during actuation and expected 100 deg angular displacement was verified.

3.2. Thermal testing

Mechanism mockup was brought into a vacuum chamber, installed on a heat-sink copper plate with liquid nitrogen cooling loop. In Fig. 12a the test setup is shown. The mechanism was mounted on two aluminum supports directly linked to the cooling plate. To monitor the temperature inside the chamber three Pt100 RTD were placed on the cold plate and on the mechanism supports. The system was cooled down to $-120\ ^{\circ}C$ and during temperature raising, current provided to the motor and temperatures were monitored. To avoid motor heating due to a continuous powering, each switch-on session was limited to 10 s. Fig. 12b shows testing results.

Below $-55\ ^{\circ}C$ the motor drains the maximum admissible current of 210 mA but does not move. The Portescap motor had a lubricated gearbox and the lubricant was expected to freeze around $-50\ ^{\circ}C$ so, this result was expected. However, if the motor was heated so that its temperature was above $-50\ ^{\circ}C$, the mechanism would be able to provide correct working.

Thus, pre-warming strategy was assumed as the baseline for the mechanism operation, despite the type of motor selected for flight was different from the breadboard one and the lubricant was expected to allow operation down to $-70\ ^{\circ}C$.

3.3. Environmental testing

The cover mechanism mockup was mounted on the instument to perform environmental testing as required in [2]. Excitation was provided by a LDS V830 SPA-16 electrodynamic shaker with LMS SCADAS III controller as shown in Fig. 13a. Response was measured by means of a triaxial accelerometer mounted on the top of the instrument optical bench. Before and after each high level test, “resonance searches” were carried out to identify possible instrument

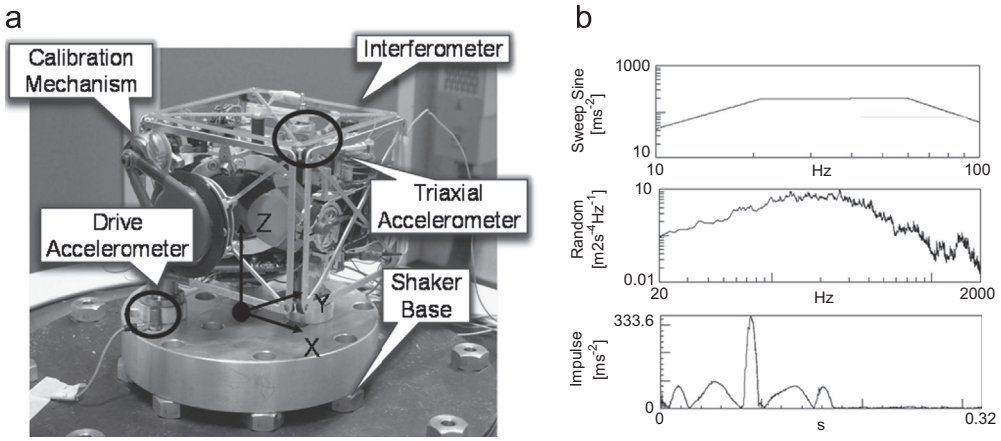

Fig. 13. (a) Mechanical testing setup: interferometer is mounted on the shaker base plate. Mechanism is mounted on the interferometer in closed position. (b) Sweep sine, random and impulse responses.

damages. Fig. 13b shows *Z* axis loading responses, respectively, for the sweep sine, random and impulse excitations.

MIMA mockup passed the qualification tests and the mechanism as well, since after testing no damages or working anomalies were detected.

4. Conclusions

An innovative roto-translational mechanism has been conceived and designed by means of FE and multibody modelling; the latter gave useful information about mechanism sensitivity to parameter changes, friction in particular. Designed mechanism allowed to perform the required movement, enabling the correct positioning of the calibration source for a miniaturized infrared spectrometer and providing the sealing of the instrument entrance window against dust and external contamination. Beside movement complexity, the main challenges came from size and mass budgets, considering that the overall system had to stay within the 30 g mass allocation.

Measured performances after mechanical and thermal tests proved its compatibility with the expected environments. The most critical point, i.e. motor performances at low temperature, was temporarily addressed with the warming-up of the motor itself to the minimum operating temperature of $-50\,^{\circ}C$. Qualification to lower operating temperature of a different type of motor was foreseen to avoid the need of the warm-up strategy.

References

[1] Debei, S De Cecco, M., Parzianello G., Francesconi A., Angrilli F.,Design, qualification and acceptance of the front door mechanisms for the Osiris experiment of Rosetta missionProceedings of SPIE2002.
[2] ExoMars Pasteur Payload Experiment Interface Requirements, Document EXM-PL-IRD-ESA-00001 Issue 6.
[3] B. Saggin, D. Scaccabarozzi, Design and optimization of the calibration procedure for a miniaturized Fourier transform spectrometer, Appl. Spectrosc. 65 (2011) 6.
[4] ECSS E30 Part 2 A, Mechanical—Part 2: Structural, ESA.
[5] ECSS E30 Part 3 A, Mechanical—Part 3: Mechanisms, ESA.
[6] L. Comolli, B. Saggin G. Bellucci, MIMA-POLIMI-TR11, LW Calibration Testing, 2009.
[7] Smalley catalogue, ⟨http://www.smalley.com/pdfs/CMCC-08.pdf⟩.
[8] Vespel Properties Guide, ⟨http://www2.dupont.com/Vespel/en_US/assets/downloads/vespel_s/233630a.pdf⟩.
[9] 08G61_BrushDC_63_v6.09.pdf, ⟨http:/www.portescap.com/BrushDC⟩.